CARBON 87 (2015) 116–127

Available at www.sciencedirect.com

ScienceDirect

journal homepage: www.elsevier.com/locate/carbon

# An advanced electrocatalyst with exceptional eletrocatalytic activity via ultrafine Pt-based trimetallic nanoparticles on pristine graphene

*Jian Zhao* [a,b,c,*], *Hongqi Li* [a], *Zhensheng Liu* [a], *Wenbin Hu* [a], *Changzhi Zhao* [a], *Donglu Shi* [b,c,*]

[a] *Key Laboratory of Rubber-Plastics Ministry of Education/Shandong Provincial Key Laboratory of Rubber-Plastics, Qingdao University of Science and Technology, No. 53 Zhengzhou Road, Qingdao 266042, China*

[b] *Shanghai East Hospital, The Institute for Biomedical Engineering & Nano Science (iNANO), Tongji University School of Medicine, Shanghai, China*

[c] *The Materials Science and Engineering Program, Department of Mechancical and Materials Engineering, College of Engineering and Applied Science, University of Cincinnati, 2600 Clifton Ave., Cincinnati, OH 45221, USA*

ARTICLE INFO

*Article history:*
Received 24 October 2014
Accepted 19 January 2015
Available online 24 January 2015

ABSTRACT

It has been a great challenge to directly deposit uniform metal particles onto pristine graphene due to its low surface energy and chemical inertness. Without any surfactant or functionalization, we have developed a unique synthesis of high-quality PtRuNi trimetallic nanoparticles supported on pristine graphene via a simple but effective supercritical route. Due to excellent wettability between supercritical carbon dioxide and the carbon surface, ultrafine metal particles are uniformly and firmly anchored on the graphene sheets. While well retaining its intrinsic structure and outstanding electronic conductivity, the pristine graphene with well-dispersed PtRuNi trimetallic nanoparticles shows significantly improved catalytic activity towards methanol oxidation, which is at least ten times higher than those of the commercial Pt/C and homemade Pt/XC-72 catalysts. The resulting trimetallic hybrid also exhibits high stability as compared to Pt and PtRu/pristine graphene composites and the reduced graphene oxide counterparts. In principle, the supercritical method can be applied to other metal nanoparticles in fabrication of high-performance graphene-based nano-catalysts.



## 1. Introduction

Recently, extensive research has been focused on direct methanol fuel cells (DMFCs) for their low pollutant emission, high energy-conversion efficiency, and easy handling and distribution [1]. To date, the most promising anode catalyst for methanol oxidation has been platinum [2]. However, commercial Pt-based fuel cells have been limited by their toxicity of

* *Corresponding authors at:* Key Laboratory of Rubber-Plastics Ministry of Education/Shandong Provincial Key Laboratory of Rubber-Plastics, Qingdao University of Science and Technology, No. 53 Zhengzhou Road, Qingdao 266042, China (J. Zhao), The Materials Science and Engineering Program, Department of Mechancical and Materials Engineering, College of Engineering and Applied Science, University of Cincinnati, 2600 Clifton Ave., Cincinnati, OH 45221, USA (D. Shi). Fax: +86 0532 84022725.

E-mail addresses: zhaojian@gmail.com (J. Zhao), donglu.shi@uc.edu (D. Shi).

http://dx.doi.org/10.1016/j.carbon.2015.01.038
0008-6223/

carbon monoxide, high cost of platinum, and catalyst particle aggregation. The addition of transition metals such as Ru to Pt-based catalysts can significantly improve the CO-tolerance in methanol electrooxidation through the so-called bifunctional mechanism and lower the overpotential [3–5]. The critical issues to be addressed by the current research involve enhancing the electrocatalytic performance of the binary PtRu alloy and reducing the costs of noble metals [6]. Recent advances on ternary catalysts by addition of nickel such as PtRuNi catalysts include improved electrocatalytic performance with an atomic ratio of 6:3:1 for methanol oxidation in comparison to the commercial Pt-based catalysts [7,8].

In order to maximize the catalytic activity of noble metals while minimizing their consumption, synthesizing Pt and Pt-based alloy nanocrystals with ultrafine sizes is a viable approach. The most effective strategy is to disperse noble metal nanoparticles on the surfaces of supporting materials [9]. One of the major requirements for an ideal supporting material is a large surface area for fine dispersion of catalyst nanoparticles. It also requires high inertness in harsh electrochemical conditions, low cost, and high electrical conductivity [10]. At present, carbon black is the most popular carbon support for catalysts. However, it has a poor corrosion tolerance in working conditions of DMFCs. It is, therefore, important to identify appropriate supporting materials and develop effective synthetic routes for improved DMFCs [1].

Currently, graphene-based materials with a unique two-dimensional honeycomb carbon substrate for immobilizing noble metal nanocrystals have been utilized in the development of high-performance electrocatalytic devices [11]. Graphene is well known for its large surface area, structural stability, excellent mechanical strength, exceptionally high electrical and thermal conductivity [12]. The methods of hybridizing graphene with noble metals have been developed by using graphite oxide (GO) sheets as a carbon precursor [9,13–16]. Oxygen functionalities on GO surfaces provide good exfoliation of the graphene sheets in some solvents and facilitate growth of metal nanoparticles. By interrupting the periodicity of $sp^2$-hybridized carbon atoms, however, the surface functionalization substantially impairs the electrical and mechanical properties of the material. Even under the strongest reducing condition, the complete removal of functionalities is impossible, as demonstrated by theoretical predictions and experimental studies [7,8]. Furthermore, numerous framework defects and defective graphene fragments remain on graphene surfaces upon reduction, leading to severe disruption of its intrinsic electronic transport. These imperfections can render the graphene-based composites considerably unstable under harsh electrochemical conditions as the defective sites usually initiate the corrosion of carbon materials [11].

As is well known, the surface of graphene is inactive due to high graphitization. As a result, it is extremely difficult to achieve direct deposition of highly dispersed metal nanoparticles on pristine graphene surfaces [1]. There have been few reports on successful preparation of pristine graphene-based metal nanoparticles. In previous studies, we showed uniform distributions of Pt or PtRu alloy on thermally reduced graphene (TRG) (or the so-called functionalized graphene sheets) via a supercritical carbon dioxide ($CO_2$) route at 120 °C or 200 °C (for the reduction of metal precursors by methanol or hydrogen) [17,18]. TRG exhibits a high density of defects that are formed during thermal expansion of GO. These defects can serve as the anchoring sites for growth of the metal nanoparticles.

In this work, we report the direct deposition of Pt, PtRu and PtRuNi nanoparticles on pristine graphene by a modified supercritical carbon dioxide route. In this synthesis, dimethyl amine borane (DMAB, a chemical hydrogen storage material [19]) replaces $H_2$ as a reducing agent. This greatly simplifies experimental setup and operation that was previously used for $H_2$. The reduction of metal precursors occurs at significantly lowered temperature (50 °C) [20,21]. Pt(II), Ru(III) and Ni(III) acetylacetonate were employed as metal precursors. The unique features of supercritical fluids include near zero surface tension, gas-like diffusion rate, and low viscosity. Under the supercritical condition, ultrafine metal nanoparticles were homogenously decorated on highly conductive graphene sheets. For comparison, reduced graphene oxide (RGO) and Vulcan XC-72 (Vulcan XC-72 from Cabot) were also investigated as support materials in the development of PtRuNi, PtNi and Pt catalysts. The pristine graphene-based composites exhibit significantly enhanced electron transport, and improved activity and stability for methanol electro-oxidation. The graphene-supported PtRuNi hybrid as an electrocatalyst shows an activity at least by a factor of ten in comparison to the commercial and home-made Pt/XC-72 catalysts, preceding any results of graphene-based Pt or Pt alloy reported in literature.

## 2. Experimental section

### 2.1. Materials

Carbon black with a specific surface area (BET) of 250 $m^2/g$ was purchased from Cabot (Vulcan XC-72). Natural Graphite Powder was obtained from Qingdao Ruisheng Graphite Co. Ltd. (purity 99.99%, particle size 40 μm). A platinum precursor ($Pt(acac)_2$, acac = acetylacetonate), a ruthenium precursor ($Ru(acac)_3$) and a nickel precursor ($Ni(acac)_3$) were purchased from Alfa Aesar. $CO_2$ was provided by Qingdao Heli Gas Co. Ltd. DMAB was obtained from Aldrich. All other chemicals were of analytical grade and used as received. Commercial Pt/C catalyst (20 wt% Pt) was purchased from Alfa Aesar.

### 2.2. Preparation of graphite oxide

Graphite oxide was prepared from natural graphite powder by the method described by Hummers et al. with some modifications [22,23]. Briefly, 5 g of graphite powder and 3.75 g of $NaNO_3$ were added to 230 mL of concentrated $H_2SO_4$ (98%) with stirring in an ice-water bath. Then, 15 g of $KMnO_4$ was slowly added over about 1 h, so that the temperature of the mixture was maintained below 10 °C. After the mixture was stirred at 35 °C for 5 days, 500 mL of 5 wt% $H_2SO_4$ aqueous solution was added over 1 h under magnetic stirring, and the temperature was kept at 98 °C for 2 h. Then, the tempera-

ture was reduced to 60 °C, 15 mL of 30 wt% $H_2O_2$ solutions was added, and the mixture was stirred for 2 h at 30 °C. The collected precipitates were washed repeatedly with 3 wt% $H_2SO_4$/0.5 wt% $H_2O_2$ solution, 5 wt% HCl aqueous solution and distilled water. Finally, the products were dried in a vacuum oven at 40 °C for three days.

### 2.3. Synthesis of graphene sheets

Graphene sheets were prepared by dispersion and exfoliation of bulk graphite in NMP based on Coleman's work [24]. Specifically, natural graphite (1 g) was dispersed in NMP (100 mL) using a sonic tip at 150 W for 2 h. The resultant suspension was then centrifuged for 2 h at 600 rpm. The top 85% of the dispersion (about 85 mL of 100 mL of the suspension) was collected by a pipette. The homogeneous dark dispersion was filtered through a nylon membrane (pore size 0.45 μm) and washed with methanol several times, followed by drying in vacuum at 50 °C to obtain graphene sheet thin film.

### 2.4. Synthesis of catalysts

The PtRuNi (with an atomic ratio of 6:3:1)/graphene (RGO or Vulcan XC-72), PtRu (with an atomic ratio of 1:1)/graphene (RGO or Vulcan XC-72) and Pt/graphene (RGO or Vulcan XC-72) catalysts, were obtained by chemical reduction with dimethyl amine borane as the reducing agent. $Pt(acac)_2$ (acac = acetylacetonate), $Ru(acac)_3$ and $Ni(acac)_3$ were used as the corresponding precursors. In a typical experiment, 20 mg of pristine graphene sheets was ultrasonically dispersed in 6 mL of a mixed solvent of methanol/NMP (volume ratio = 1:2) for 1 h. Then 20 mg of dimethyl amine borane, 20 mg of $Pt(acac)_2$, certain amount of $Ru(acac)_3$ or $Ni(acac)_3$ were added to the ink and then mixed thoroughly for 30 min. Then the suspension was loaded in a 25 mL stainless autoclave. The autoclave was sealed and $CO_2$ was charged into the vessel up to 16 MPa in an oven at 50 °C in order to obtain a supercritical fluid. The system was stirred vigorously for 4 h before the vessel was depressurized. Catalyst powder was collected after sonicating and washing 5 times using methanol. The produced sample was vacuum-dried at 50 °C for 24 h. Similarly, Vulcan XC-72-based composites were prepared under the same experimental conditions. RGO-based composites were initially prepared under the same supercritical conditions (at 50 °C) using GO as the starting material. However, the reduction degree of GO was low so that no significant electrocatalytic activity was measured. The reaction temperature was elevated to 180 °C to fully reduce GO (the dispersion of metal nanoparticles on RGO would not be influenced at this temperature) [25].

### 2.5. Electrocatalytic property measurements

The electrochemical properties of the resulting composites were characterized by cyclic voltammogram (CV) and chronoamperometry (CA) using a conventional three-electrode cell on a CHI660B Electrochemical Workstation (Chenhua, China). All tests were conducted at room temperature. A glass carbon electrode coated with catalysts (3 mm in diameter) was used as the working electrode, a Pt wire as counter electrode, and Ag/AgCl electrode as reference electrode. 10 μL of N,N-dimethylformamide solution containing catalyst (2.5 mg/mL) was cast dropwise onto glass carbon electrode surface. After drying at room temperature in air, 8 μL of 0.05 wt% Nafion solution was dropped on the surface of the catalyst layer to form a thin film, preventing catalyst from detaching. Prior to the electrochemical tests, the working electrode was dried for 3 h at room temperature. The electrocatalytic activity and stability of the catalysts for the oxidation of methanol were evaluated in 1 M $CH_3OH$ and 0.5 M $H_2SO_4$ by means of CV and CA tests. The electrolyte solutions were deaerated with ultrahigh purity nitrogen for 15 min prior to any measurement.

The impedance spectra were obtained on SI 1260 impedance/gain-phase analyzer at frequencies from 100 kHz to 0.01 Hz with amplitude of 5 mV at a potential of −0.15 V (vs. Ag/AgCl), and ZPlot and ZView softwares were used to measure and analyze the impedance data, respectively.

### 2.6. Characterization

The composites were dispersed with a mixed solution of 5 mL of HCl (2.1 M) and 5 mL of $HNO_3$ (2.1 M) in a block tube heated at 95 °C for 4 h [26–28]. After maintaining at room temperature for 12 h, 2 mL of HF was added. The sample solutions were digested at 95 °C for 2 h. Inductively coupled plasma spectroscopy/optical emission spectroscopy (ICP/OES, Perkin–Elmer, Optima 3300XL with AS 91autosampler) was used to analyze the resulting solutions for the metal contents of the prepared composites.

X-ray diffraction (XRD) patterns were obtained using a D-MAX 2500/PC operated at 40 kV and 100 mA with Cu Kα radiation ($\lambda$ = 0.15418 nm). The X-ray photoelectron spectroscopy (XPS) measurement of the composites was performed on a RBD upgraded PHI-5000C ESCA system (Perkin Elmer) with Al Kα radiation (hν = 1486.6 eV). The data analysis was carried out using RBD Augerscan 3.21 software (RBD Enterprises, USA). Raman spectroscopy was performed on a Renishaw inVia Raman System 1000 with a 532 nm Nd:YAG excitation source at room temperature. The morphologies of the composites were examined by a JEOL 2010 transmission electron microscope (TEM) equipped with an energy-dispersive X-ray spectrometer (EDS).

## 3. Results and discussion

Typical XRD patterns of dried graphene, PtRuNi/graphene, PtRu/graphene, and Pt/graphene composites are presented in Fig. 1a. As can be seen in XRD pattern of dried graphene, the predominant and sharp diffraction peak at 26.5° is evidently attributed to the (002) plane reflection of crystallized hexagonal graphite. A minor diffraction peak at 54.7° can be assigned to (004) plane of hexagonal graphite. These features suggest that the exfoliated graphene sheets were restacked with each other upon drying in the oven.

We observed significant decreases in the intensity of characteristic peaks of the (002) plane reflection of graphene in

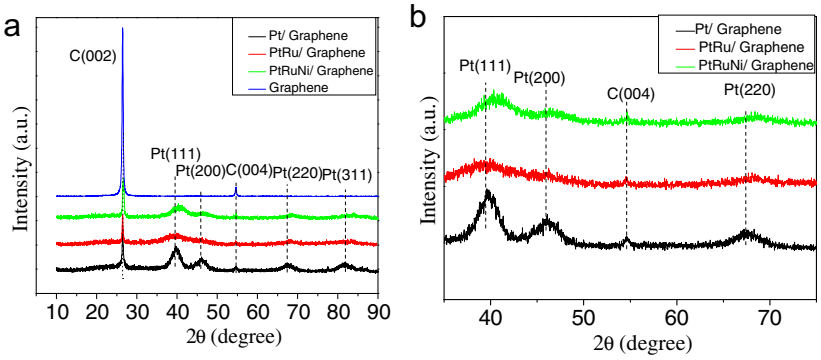


**Fig. 1 – (a) Wide scanning of XRD diffractions of dried graphene, PtRuNi/graphene, PtRu/graphene and Pt/graphene samples; (b) magnified XRD patterns of PtRuNi/graphene, PtRu/graphene and Pt/graphene samples. (A color version of this figure can be viewed online.)**

the XRD patterns of PtRuNi/graphene, PtRu/graphene and Pt/graphene composites. This behavior is due to reduced aggregation and restacking of graphene sheets by the attached metal nanoparticles. The four other peaks, characteristic of the face centered cubic (fcc) crystalline Pt (JCPDS card No. 65-2868), correspond to the planes (111), (220), (200), and (311), respectively.

The alloy catalysts display a dominant feature of disordered single-phase structures. As compared to the diffraction peaks of Pt/graphene, those of PtRuNi/graphene and PtRu/graphene are shifted to higher $2\theta$ values [10,29]. The (111) peaks of PtRuNi/graphene and PtRu/graphene are both shifted over 39.61° for Pt/graphene. Those of PtRuNi/graphene and PtRu/graphene are at 41.31° and 40.36°, respectively, as can be seen in Fig. 1b. The same trend is also found for the (220) peaks [67.24° (Pt), 68.10° (PtRu), 68.41° (PtRuNi)]. The peak shift to the higher angle for Pt accounts for the alloy formation between Pt, Ru, and Ni. By fitting the (220) peak, the d spacing of (220) in the PtRuNi and PtRu alloy nanoparticles are respectively 1.3704 Å, and 1.3757 Å, whereas that of pure Pt is 1.3912 Å. Clearly, among three catalysts, the d spacing of (220) for PtRuNi/graphene is the smallest, while that of Pt/graphene is the largest. The lowered lattice parameters for the alloy hybrids indicate the progressive increase in incorporation of Ni and Ru atoms into the alloy. PtRu is known for high solubility in the binary system. The metallic Ni and Ru atoms are likely in the platinum lattice of PtRuNi alloy, and the metallic grains containing Ni are intermixed with amorphous Ni oxides, such as $Ni(OH)_2$, NiO, and NiOOH (see XPS data below). Another possibility is the presence of oxides at the grain surfaces.

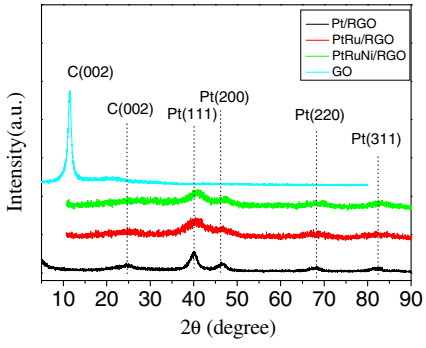


**Fig. 2 – XRD patterns of GO, PtRuNi/RGO, PtRu/RGO and Pt/RGO samples. (A color version of this figure can be viewed online.)**

Fig. 2 shows XRD patterns of GO, PtRuNi/RGO, PtRu/RGO and Pt/RGO composites. The most intensive speak at $2\theta = 11.1°$ corresponds to the (002) reflection of GO. The interlayer spacing (0.80 nm) is larger than that of pristine graphite (0.34 nm) due to introduction of the oxygen-containing groups (hydroxyl, epoxy, carboxyl and carbonyl groups) [21]. In the cases of composites, the (002) reflection peak of layered graphite oxide disappears and no prominent peaks corresponding to graphene aggregates are found. Although GO was reduced during the preparation of the composites, the stacking of the reduced graphene oxide was fully inhibited by the metallic nanoparticles. The other diffraction peaks of PtRuNi/RGO, PtRu/RGO and Pt/RGO composites are assigned to metallic Pt with the similar trend of angle shift as PtRuNi/graphene, PtRu/graphene, and Pt/graphene composites.

The morphology, the size and the dispersion of the metal particles deposited on different carbon supports were studied by TEM. Fig. 3 shows the typical TEM micrographs of Pt/graphene, PtRu/graphene and PtRuNi/graphene, respectively. As can be seen from Fig. 3(a–c), the nearly transparent carbon sheets are the result of extremely thin monolayer and few-layer graphene sheets, generated during the preparation processes. In all cases, ultrafine nanoparticles are uniformly and firmly decorated on large area of graphene sheets with similar sizes. Long-term sonication did not remove the metallic particles on graphene. The particle distributions (Fig. 3d–f) are from 1.7 to 4.8 nm for Pt/graphene, 1.3 nm to 4.7 nm for PtRu/graphene and 1.7 to 4.4 nm for PtRuNi/graphene. The average particle size is 3.11 nm for Pt/graphene, 2.85 nm for PtRu/graphene and 3.02 nm for PtRuNi/graphene. This indicates minimal size influence on their catalytic activity for methanol electro-oxidation. Presented as an inset in Fig. 3(a–c), the corresponding selected area electron diffraction (SAED) patterns taken from the three composites also share structural similarities: each exhibits not only a typical sixfold symmetry diffraction pattern arising from graphene, but also characteristic Pt diffraction circles as polycrystals. No crystalline reflections of Ru or Ni species were detected.

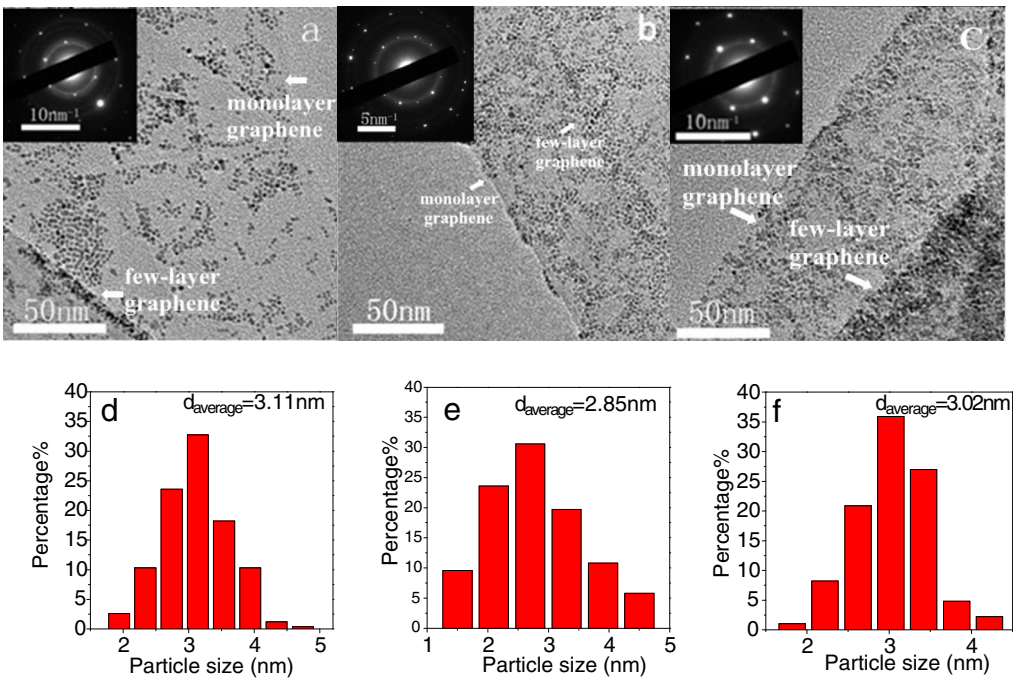


**Fig. 3 – TEM images of Pt/graphene (a), PtRu/graphene (b) and PtRuNi/graphene (c) composites with SAED patterns as insets, and the particle size distributions of Pt/graphene (d), PtRu/graphene (e) and PtRuNi/graphene (f) composites. (A color version of this figure can be viewed online.)**

Elemental identification of the nanoparticles was performed using energy-dispersive X-ray spectroscopy (EDS). EDS spectra (Fig. S1, see Supplementary Information) show the presence of Pt, Ru and Ni in PtRuNi/graphene, Pt and Ru in PtRu/graphene, and Pt in Pt/graphene. ICP analysis shows the exact contents of metals in the composites: 24.8 wt% Pt, 12.6 wt% Ru and 4.1 wt% Ni in PtRuNi/graphene, 19.2 wt% Pt and 17.7 wt% Ru in PtRu/graphene and 21.1 wt% Pt in Pt/graphene, respectively.

The uniform dispersion of metal nanoparticles on pristine graphene is attributed to the gas-like diffusivity, extremely low viscosity, and near-zero surface tension of supercritical $CO_2$. Moreover, the excellent penetration of supercritical $CO_2$ can effectively debundle (by intercalation and exfoliation) [30] graphene and distribute nanoparticles to prevent restacking of the graphene sheets. It should be pointed out that no substrate pretreatment was required to obtain the high-quality nanoparticle distribution.

In the cases of the RGO-based metal hybrids (PtRuNi/RGO, PtRu/RGO and Pt/ RGO), it is evident that the nanoparticles tend to agglomerate on RGO. RGO is rippled with a dimension of several hundred nanometers to a few microns (Fig. 4). TEM observation indicates that no RGO aggregates into layered structure, consistent with the XRD analysis. Although abundant oxygen-containing groups on GO can promote the deposition of metal particles, conglomeration of metal nanoparticles can take place due to the uneven distribution of excessive functional groups and the rough graphene surface.

For comparison, we also estimate the size distributions of the particles supported on carbon black (PtRuNi/XC-72, PtRu/XC-72 and Pt/XC-72) prepared under the same experimental conditions. Larger particles with broader size distributions are found in these samples (Fig. 5a–c). Detailed analysis shows that the average particle sizes of Pt/XC-72, PtRu/XC-72 and PtRuNi/XC-72 are 4.37 nm, 4.72 nm and 4.64 nm, respectively (Fig. 5d–f). The metal contents of carbon black

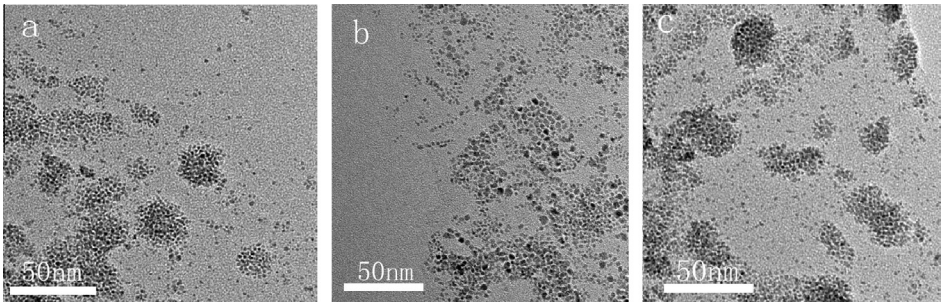


**Fig. 4 – TEM images of Pt/RGO (a), PtRu/RGO (b), and PtRuNi/RGO (c).**

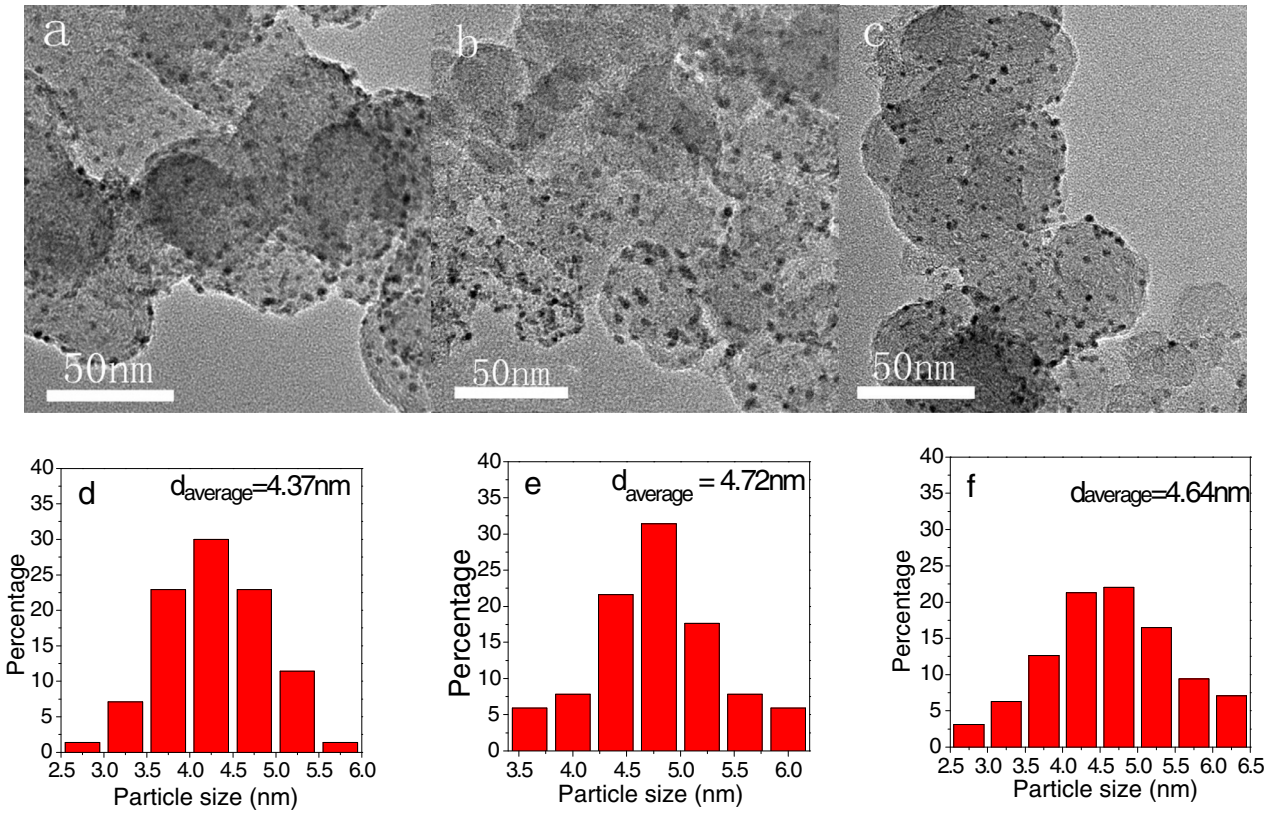


**Fig. 5 – TEM images of Pt/XC-72 (a), PtRu/XC-72 (b) and PtRuNi/XC-72 (c), and particle size distributions of Pt/XC-72 (d), PtRu/XC-72 (e) and PtRuNi/XC-72 (f). (A color version of this figure can be viewed online.)**

and RGO-based composites are listed in Table S1 (see Supplementary Information), as determined by ICP digestion. The morphology and size of the commercial Pt/C are shown in Fig. S2.

Raman spectroscopy was utilized to evaluate structural defects and number of layers of the graphene-based samples [31]. Fig. 6 shows the Raman spectra of pristine graphene, Pt/graphene, PtRu/graphene, PtRuNi/graphene. The appearance of three major peaks at approximately 1350 $cm^{-1}$, 1580 $cm^{-1}$ and 2700 $cm^{-1}$ are assigned to the D band, G band and 2D band of graphene, respectively [32]. The D band is caused by

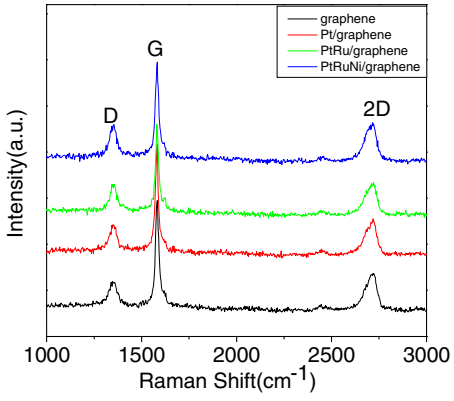


**Fig. 6 – Raman spectra of pristine graphene, Pt/graphene, PtRu/graphene and PtRuNi/graphene. (A color version of this figure can be viewed online.)**

the structural disorder or defects ($sp^3$ bonds), while the G-band corresponds to the doubly degenerate $E_2g$ mode of graphite which is related to the coplanar vibration of $sp^2$ carbon atoms in a two-dimensional hexagonal lattice. The 2D band arises from second-order zone boundary phonons and shifts according to the number of graphene layers [33,34]. For pristine graphene, the intensity ratio ($I_D/I_G$) of the D to G band is small (0.19), indicating low defect density of graphene [35]. For the graphene-based samples, the intensity ratio ($I_D/I_G$ = 0.21, 0.24 and 0.23 for Pt/graphene, PtRu/graphene and PtRuNi/graphene, respectively) only increases slightly, confirming highly crystalline structure of graphene upon supercritical $CO_2$-assisted deposition of the metal nanoparticles. The integrity of graphene is critical for achieving good electrical conductivity and high electrocatalytic performance of the composites. The line shape and position (at around 2708 $cm^{-1}$) of 2D band in the Pt/graphene, PtRu/graphene and PtRuNi/graphene composites indicates the few-layer graphene structure in the composites [31,36].

Significant structural changes occurred during the chemical processing as GO transforms to RGO nanosheets. Fig. 7 shows Raman spectroscopy result of pure graphite. As can be seen in this figure, D and G modes are weak, but after oxidation both modes become wider with increased intensity. The well defined 2D band peak (2725 $cm^{-1}$) of pure graphite begins to change in the GO spectrum as shown in Fig. 7. The G bands of the RGO-based composites are also broadened and upshifted in comparison to those observed in graphite (from 1583 $cm^{-1}$ for graphite to 1595 $cm^{-1}$ for Pt/RGO,

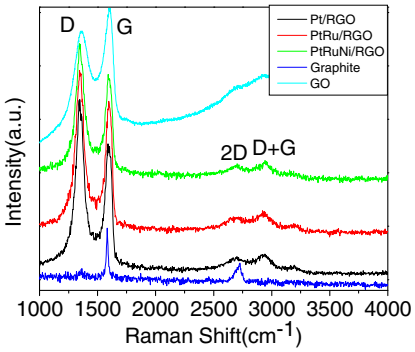


**Fig. 7 – The Raman spectra of pure graphite, GO, Pt/RGO, PtRu/RGO and PtRuNi/RGO. (A color version of this figure can be viewed online.)**

1593 $cm^{-1}$ for PtRu/RGO and 1592 $cm^{-1}$ for PtRuNi/RGO). A possible explanation for this behavior is the presence of isolated double bonds which resonate at higher frequencies [37]. Furthermore, the D band at 1346 $cm^{-1}$ becomes prominent, indicating the presence of structural imperfections generated by the attachment of hydroxyl and epoxide groups on the carbon plane [33]. Once formed, these defects become very difficult to remove even by strong reducing reagents. The D/G intensity ratios ($I_D/I_G$) of the RGO-based samples show enhanced values as compared to that of GO ($I_D/I_G = 0.85$), indicating more $sp^2$ domains with a decreased average size upon reduction of GO [21,38,39]. Compared with pristine graphene-based composites, the intensity of D band significantly increases (relative to G band), implying reduced electrical conductivity [40,41]. The additional peaks of overtone (2D) and combination bands (D + G) associated with the local disorder and defects in the $sp^2$ phase are also seen in the Raman spectra of the RGO-based composites, consistent with previous observations of graphene–metal composites [42,43]. The peak position (around 2691 $cm^{-1}$) of the 2D band is similar to that of a monolayer graphene [31,36].

XPS was used to determine the surface elemental composition and covalent state of various species in the graphene-based catalysts. The Pt 4f spectrum of Pt/graphene is shown in Fig. 8(a). Strong doublet peaks at 71.22 eV (Pt $4f_{7/2}$) and 74.46 eV (Pt $4f_{5/2}$) with the theoretical ratio of peak areas of 4:3 indicate the element Pt [44]. The other two weaker doublets correspond to Pt oxides. The doublet peaks at 72.26 and 76.99 eV can be attributed to $Pt^{2+}$ in the form of PtO or $Pt(OH)_2$, while the doublet peaks at 75.60 and 78.59 eV arises from $Pt^{4+}$, possibly in the form of $PtO_2$ [44]. Detailed XPS analysis shows that Pt is comprised of 73.1 % metallic Pt, 14.6% PtO or $Pt(OH)_2$, and 12.3% $PtO_2$.

Fig. 8(b) and (c) shows the Pt 4f and Ru 3p spectra of the PtRu/graphene composite, respectively. The Pt $4f_{7/2}$ and $4f_{5/2}$ lines appear at the binding energies of 71.13 eV (Pt $4f_{7/2}$) and 74.30 eV (Pt $4f_{5/2}$). Compared to Pt/graphene, their positions are shifted to lower binding energy due to ruthenium addition [6]. Pt electronic modification by less or smaller electronegative metal atoms originates from the strain experienced by Pt atoms residing on top of atoms with a smaller Wagner-Sweitz radius or partial charge transfer [45–49]. The other two weaker doublets are assigned to Pt oxides (Fig. 8b). The Pt 4f XPS spectrum of PtRu/graphene shows that Pt contains 80.8% of metallic $Pt^0$, 10.0% of $Pt^{2+}$ (as PtO or $Pt(OH)_2$), and 9.2% of $Pt^{4+}$ (as $PtO_2$). The main Ru $3p_{3/2}$ peak is deconvoluted into two distinguishable peaks at 462.45 and 465.29 eV, which are attributed to Ru (0) and $RuO_2$, respectively [50,51]. The calculation shows that Ru contains 84.2% of metallic state $Ru^0$, while a much smaller fraction (about 15.8%) exists as $RuO_2$. Based on the bifunctional mechanism, more oxophilic metal such as Ru covered by RuOH is the source of oxygen required for removal of absorbed surface CO intermediate. As a result, PtRu has excellent catalytic activity as compared to pure Pt [52].

The Pt 4f, Ru 3p and Ni 2p XPS spectra of the PtRuNi/graphene composite are shown in Fig. 8(d)–(f), respectively. Similar to those of the PtRu/graphene composite, the most intense doublet peaks are found at the binding energies of 70.97 eV (Pt $4f_{7/2}$) and 74.21 eV (Pt $4f_{5/2}$). In comparison with the PtRu/graphene composite, a notable XPS shift is observed in the PtRuNi/graphene composite, consistent with greater difference in the electronegativity between Ni and Pt and that between Ru and Pt [6]. The bond energy between Pt and $CO_{ads}$ can be decreased due to electron transfer from Ni to Pt via reduction of DOS at the Fermi level during methanol electro-oxidation [46]. This partly explains improved eletrocatalytic performance in the PtRuNi/graphene composite (see electrocatalytic results). The deconvolution of the XPS spectra of Pt 4f gives a phase composition of 76.0% of Pt in metallic $Pt^0$, 12.9% in $PtO_2$, and 11.1% in PtO or Pt $(OH)_2$. Based on the Ru 3p spectrum, 67.7% of metallic Ru and 32.3% of $RuO_2$ are contained in the element Ru.

In the PtRuNi ternary nanoparticles, the Ni states consist of Ni metal ($Ni^0$) as well as Ni oxide and hydroxides (NiO, $Ni(OH)_2$, and NiOOH) as shown in Fig. 8(f) [6]. The peaks at 852.30, 853.84, 855.60 and 857.76 eV can be attributed to the metallic $Ni^0$, NiO, $Ni(OH)_2$ and NiOOH with the contents of 22.5%, 23.3%, 14.8%, and 14.5%, respectively. As shown in the XRD results, the metallic Ni atoms can interstitially insert into the Pt lattice. The remarkable binding energy shift for Pt, as identified by XPS, originates from the modification of electronic structure of platinum by electron transfer from Ni to Pt. As a result, the Pt–CO bond energy is lowered, facilitating surface CO removal and leading to improved activity of PtRuNi/graphene for methanol electrooxidation (see CV results). Moreover, it has been demonstrated that the nickel hydroxides (NiOOH and $Ni(OH)_2$) possess high proton and electron conductivity, and capable of oxidizing methanol in acid or alkaline solution [53]. The hydroxide layer is well protected from corrosion under electrochemical conditions [6]. Meanwhile, Ni hydroxides can play a significant role in the shift of Hads on Pt surface which leads to the so-called hydrogen spillover effect [6,54].

Similar trend of Pt 4f peak shift is found in Pt/RGO, PtRu/RGO and PtRuNi/RGO (data not shown). Fig. S3 shows the C 1s XPS spectra of GO and PtRuNi/RGO. The intensities of the –C–OH (286.6 eV), –C–O–C–(287.4 eV) and –COOH (288.8 eV) groups in the C 1s XPS spectrum of PtRuNi/RGO significantly decrease as compared with the peaks of GO, indicating deoxygenation of GO [55].

To investigate the potential application of the composites as effective electrocatalysts for methanol oxidation, the CV

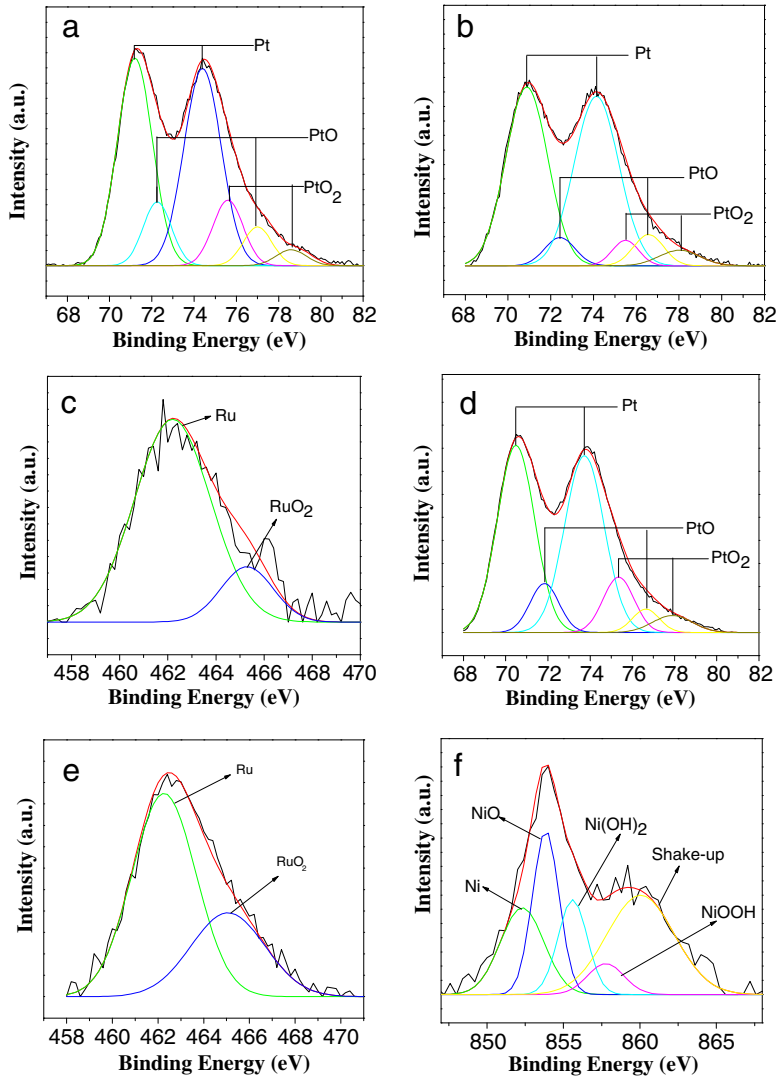


**Fig. 8 – (a) Pt 4f spectrum of Pt/graphene, (b) Pt 4f spectrum and (c) Ru 3p spectrum of PtRu/graphene, (d) Pt 4f spectrum, (e) Ru 3p spectrum and (f) Ni 2p spectrum of PtRuNi/graphene composite. (A color version of this figure can be viewed online.)**

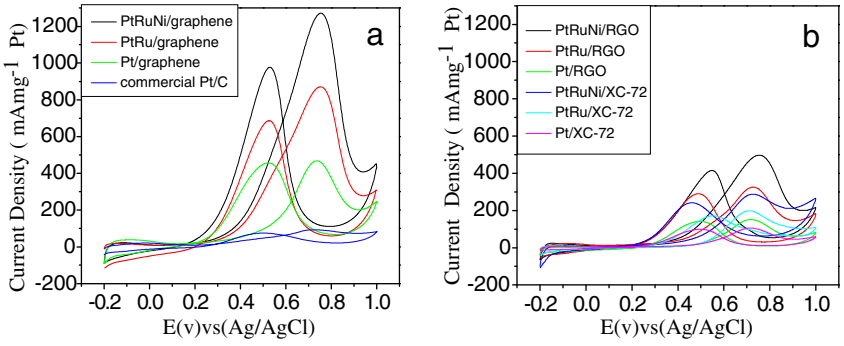


**Fig. 9 – (a) Cyclic voltammograms of the commercial Pt/C, Pt/graphene, PtRu/graphene and PtRuNi/graphene; (b) cyclic voltammograms of the Pt/RGO, PtRu/RGO, PtRuNi/RGO, Pt/XC-72, PtRu/XC-72 and PtRuNi/XC-72 in the mixed solution of 1 M $CH_3OH$ and 0.5 M $H_2SO_4$ at a scan rate of 20 mV $s^{-1}$. (A color version of this figure can be viewed online.)**

curves were obtained in a solution of 0.5 M $H_2SO_4$ and 1 M $CH_3OH$ at 20 mV/s between 0 V and +1.0 V. As shown in Fig. 9a and b (the CVs in 0.5 M $H_2SO_4$ in the absence of $CH_3OH$ are shown in Fig. S4), each of the curves includes a similar methanol oxidation peak at around 0.7–0.8 V during the positive potential excursion and another anodic peak during the subsequent negative excursion associated with the removal of incompletely oxidized carbonaceous species such as CO

formed during the positive potential excursion. The calculated mass activities (Fig. 9a) of PtRuNi/graphene, PtRu/graphene and Pt/graphene reach 1271.4, 872.9 and 468.6 mA/mg Pt. By comparison, these activities are 13.8 times, 9.6 times and 5.4 times, respectively, as high as that of the commercial Pt/C (91.9 mA/mg Pt). Further comparisons (Fig. 9b) indicate that the activities of PtRuNi/graphene, PtRu/graphene and Pt/graphene are at least twice as large as the corresponding RGO-based counterparts (497.6 mA/mg Pt for PtRuNi/RGO, 327.4 mA/mg Pt for PtRu/RGO and 152.2 mA/mg for Pt/RGO) and four times the corresponding homemade carbon black-based counterparts (286.6 mA/mg Pt for PtRuNi/XC-72, 197.2 mA/mg Pt for PtRu/XC-72 and 107.8 mA/mg for Pt/XC-72). These significant improvements are the result of uniform distribution of metal nanoparticles on the 2D carbon material, and the retained electrical conductivity of pristine graphene. The addition of Ni also considerably enhances the electrocatalytic performance towards methanol oxidation (see the XPS analysis discussed above).

The pristine graphene with well-dispersed PtRuNi trimetallic nanoparticles shows exceptional electrocatalytic activity for methanol oxidation, much higher than those of the state-of-art Pt-based nanomaterials such as PVP-modified carbon nanofibers or carbon nanotubes (CNTs)-supported PtRu nanoparticles (716.0 mA/mg Pt for nanofibers or 528.5 mA/mg Pt for CNTs) [56], CNTs/ionic liquid/PtRu hybrids (242.3 mA/mg Pt) [57], CNT/Pt composite catalysts (164.0 mA/mg Pt) [56,58], and polyaniline/Pt hybrid (45.9 mA/mg Pt) [59]. For comparison, some recently reported state-of-art Pt or Pt alloy electrocatalysts supported on graphene sheets (or with CNTs) are listed in Table S2. There have been great efforts on producing high performance heterostructure with well-controlled dimensions, morphologies, and the effective loading of Pt or alloy on graphene sheets [1]. But as demonstrated in this study, the simple combination of pristine graphene and PtRuNi trimetallic nanoparticles can far outperform any of the graphene-based Pt or Pt alloy reported in literature in terms of mass activity [16,60–63]. First, an electronic conductive support can facilitate electron transfer from a support to metal nanoparticles. The outstanding conductivity of pristine graphene, therefore, would make crucial contribution to the high electrocatalytic performance. On the other hand, the electrochemical property is strongly affected by the Pt or Pt alloy particle size and morphology. The optimal average spherical particle size was determined to be 3 nm that is responsible for the high methanol electro-oxidation effect [46]. In the present work, the supercritical fluid method enabled the growth of Pt-based nanoparticles with a spherical morphology and an optimal size of around 3.0 nm. In addition, no halide ions and surfactants were involved in the entire preparation process, ensuring a clean interface between the metal nanoparticles and graphene [64]. These factors further enhance the electrocatalytic activity of Pt-based metal nanoparticles in the nanocomposites.

CA experiments were carried out at a potential of 0.60 V in a solution of 0.5 M $H_2SO_4$ + 1.0 M $CH_3OH$. The corresponding current–time curves are shown in Fig. 10. The current density of the samples decays with time for all catalysts due to formation of CO and other residual carbonaceous species on the electrode surfaces. We observed the most rapid initial decay

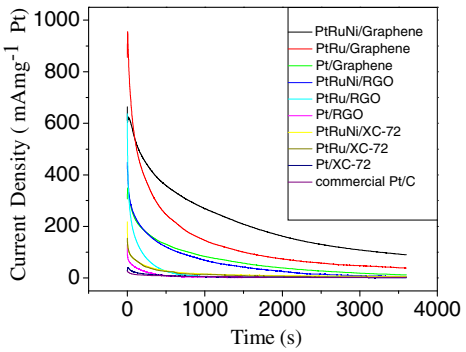


**Fig. 10 – Current–time curves of the catalysts at 0.6 V for 3600 s in a solution of 1 M $CH_3OH$ and 0.5 M $H_2SO_4$. (A color version of this figure can be viewed online.)**

in current density for carbon black-based Pt catalysts. But for the PtRuNi/graphene catalyst, the loss of the current density is significantly smaller than those of other catalysts during the initial period. Among all composites, PtRuNi/graphene has the highest current density in the entire process, showing its optimum electrocatalytic performance and stability for methanol oxidation. The current decay of the RGO and Vulcan XC-72 based composites exhibit the same trend as PtRuNi/graphene < PtRu/graphene < Pt/graphene, showing the enhanced catalytic stability for methanol oxidation by addition of Ni. It is noted that the current measured at 1 h at PtRuNi/graphene is more than one and half order of magnitude higher than those obtained with commercial Pt/C, homemade Pt/XC-72 and Pt/RGO.

The RGO-based composites exhibit poor stability since the metal nanoparticles tend to agglomerate and unevenly distribute on RGO, thus suffering from more severe intermediate carbonaceous species accumulation. Another possibility is that the high density of graphene defects in the composites can render the RGO-based catalysts to corrode easily and hence become much less stable under harsh electrochemical conditions. The enhanced stability of PtRuNi/graphene can be ascribed partly to its unique few-layer graphene structure. Once the outmost graphene layer is corroded, PtRuNi/graphene with more graphene layers can retain its base graphitized structure.

Electrochemical impedance spectroscopy was employed to determine the charge transfer resistance (Rct) during the methanol oxidation process. Fig. 11 shows the Nyquist plots of the PtRuNi/RGO, Pt/graphene, PtRu/graphene and PtRuNi/graphene catalysts obtained in a solution of 0.5 M $H_2SO_4$ + 1.0 M $CH_3OH$ at a potential of −0.15 V (vs. Ag/AgCl). The Nyquist plots of the samples contain a partially overlapped semicircle. The charge transfer resistance of the catalysts can be measured by estimating the diameter of the primary semicircle. Note that this is the only circuit element with the physical parameter describing the rate of charge transfer during the methanol oxidation reaction. The impedance data were fitted by using the ZView software and equivalent circuit [65]. The Rct values are 23.8 Ω, 26.7 Ω, 8.9 Ω and 4.8 Ω for PtRuNi/RGO, Pt/graphene, PtRu/graphene and PtRuNi/graphene, respectively. The charge transfer resistance in graphene-based PtRuNi is much lower than that in PtRuNi/

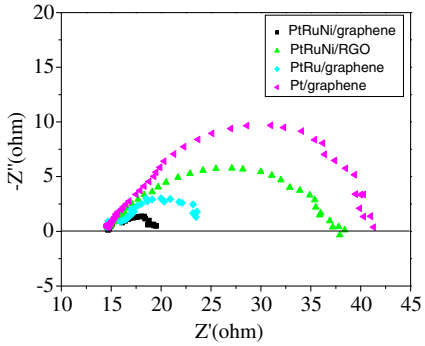


**Fig. 11 – Nyquist plots for the PtRuNi/RGO (a), Pt/graphene (b), PtRu/graphene (c) and PtRuNi/graphene (d) catalysts in a solution of 0.5 M $H_2SO_4$ + 1.0 M $CH_3OH$ at a potential of −0.15 V (vs. Ag/AgCl) at room temperature. (A color version of this figure can be viewed online.)**

RGO. That is, the highly crystalline graphene lattice plays a crucial role in promoting the electron transport [66]. The decreasing Rct value for the graphene-based catalysts indicates lowered reaction resistance of methanol electro-oxidation and enhanced catalytic activity in the order of PtRuNi/graphene > PtRu/graphene > Pt/graphene, consistent with the previously reported carbon black-based hybrids [66].

## 4. Conclusion

Without any surfactant or functionalization, highly dispersed Pt-based trimetallic nanoparticles were directly synthesized on pristine graphene by a facile supercritical method. The supercritical $CO_2$ can wet graphene surfaces and uniformly disperse the nanoparticles, which subsequently suppress graphene restacking. The structural integrity and conductivity of graphene is well preserved in the supercritical $CO_2$-assisted process. Consequently, the graphene-based composites exhibit significantly enhanced electron transport, improved stability and activity for methanol electrooxidation. The high quality graphene-supported PtRuNi hybrid as an electrocatalyst shows improved activity at least by one order of magnitude in comparison to the commercial Pt/C and homemade Pt/XC-72 catalysts, far outperforming the reduced graphene oxide-based Pt or Pt alloy hybrids. The high performance of graphene-based hybrids is found to be associated with the retained intrinsic electrical conductivity of graphene, which is critical for improving the electron transfer channels at the interfaces of graphene, metal nanoparticles, and electrolytes. These results show great potential of pristine graphene as an ideal 2-D support for the development of high-performance electrocatalysts.

## Acknowledgements

The work was supported by the National Basic Research Program of China (No. 2012CB722606) and the National Natural Science Foundation of China (No. 51373088).

## Appendix A. Supplementary data

Supplementary data associated with this article can be found, in the online version, at http://dx.doi.org/10.1016/j.carbon.2015.01.038.

## REFERENCES

[1] Huang H, Wang X. Recent progress on carbon-based support materials for electrocatalysts of direct methanol fuel cells. J Mater Chem A 2014;2(18):6266–91.
[2] Zang J, Wang Y, Bian L, Zhang J, Meng F, Zhao Y, et al. Bucky diamond produced by annealing nanodiamond as a support of Pt electrocatalyst for methanol electrooxidation. Int J Hydrogen Energy 2012;37(8):6349–55.
[3] Du B, Rabb SA, Zangmeister C, Tong Y. A volcano curve: optimizing methanol electro-oxidation on Pt-decorated Ru nanoparticles. Phys Chem Chem Phys 2009;11(37):8231–9.
[4] Maillard F, Lu GQ, Wieckowski A, Stimming U. Ru-decorated Pt surfaces as model fuel cell electrocatalysts for CO electrooxidation. J Phys Chem B 2005;109(34):16230–43.
[5] Xu W, Lu T, Liu C, Xing W. Nanostructured PtRu/C as anode catalysts prepared in a pseudomicroemulsion with ionic surfactant for direct methanol fuel cell. J Phys Chem B 2005;109(30):14325–30.
[6] Park KW, Choi JH, Kwon BK, Lee SA, Sung YE, Ha HY, et al. Chemical and electronic effects of Ni in Pt/Ni and Pt/Ru/Ni alloy nanoparticles in methanol electrooxidation. J Phys Chem B 2002;106(8):1869–77.
[7] Bagri A, Mattevi C, Acik M, Chabal YJ, Chhowalla, Manish, et al. Structural evolution during the reduction of chemically derived graphene oxide. Nat Chem 2010;2:581–7.
[8] Pei S, Cheng HM. The reduction of graphene oxide. Carbon 2012;50(9):3210–28.
[9] Zhao Y, Yang X, Zhan L, Ou S, Tian J. High electrocatalytic activity of PtRu nanoparticles supported on starch-functionalized multi-walled carbon nanotubes for ethanol oxidation. J Mater Chem 2011;21:4257–63.
[10] Martínez-Huerta M, Rojas S, Gómez De La Fuente J, Terreros P, Pena M, Fierro J. Effect of Ni addition over PtRu/C based electrocatalysts for fuel cell applications. Appl Catal B Environ 2006;69(1):75–84.
[11] Li N, Cao M, Hu C. Review on the latest design of graphene-based inorganic materials. Nanoscale 2012;4(20):6205–18.
[12] Rao CNR, Sood AK, Subrahmanyam KS, Govindaraj A. Graphene: the new two-dimensional nanomaterial. Angew Chem Int Ed 2009;48(42):7752–77.
[13] Shang N, Papakonstantinou P, Wang P, Silva SRP. Platinum integrated graphene for methanol fuel cells. J Phys Chem C 2010;114(37):15837–41.
[14] Si Y, Samulski ET. Exfoliated graphene separated by platinum nanoparticles. Chem Mater 2008;20(21):6792–7.
[15] Xu C, Wang X, Zhu J. Graphene–metal particle nanocomposites. J Phys Chem C 2008;112(50):19841–5.
[16] Zhou YG, Chen JJ, Wang FB, Sheng ZH, Xia XH. A facile approach to the synthesis of highly electroactive Pt nanoparticles on graphene as an anode catalyst for direct methanol fuel cells. Chem Commun 2010;46(32):5951–3.
[17] Zhao J, Zhang L, Chen T, Yu H, Zhang L, Xue H, et al. Supercritical carbon-dioxide-assisted deposition of Pt nanoparticles on graphene sheets and their application as an electrocatalyst for direct methanol fuel cells. J Phys Chem C 2012;116(40):21374–81.

[18] Zhao J, Zhang L, Xue H, Wang Z, Hu H. Methanol electrocatalytic oxidation on highly dispersed platinum–ruthenium/graphene catalysts prepared in supercritical carbon dioxide–methanol solution. RSC Adv 2012;2(25):9651–9.
[19] Umegaki T, Yan JM, Zhang XB, Shioyama H, Kuriyama N, Xu Q. Boron-and nitrogen-based chemical hydrogen storage materials. Int J Hydrogen Energy 2009;34(5):2303–11.
[20] Kim YT, Lee H, Kim HJ, Lim TH. PtRu nano-dandelions on thiolated carbon nanotubes: a new synthetic strategy for supported bimetallic core–shell clusters on the atomic scale. Chem Commun 2010;46(12):2085–7.
[21] Stankovich S, Dikin DA, Piner RD, Kohlhaas KA, Kleinhammes A, Jia Y, et al. Synthesis of graphene-based nanosheets via chemical reduction of exfoliated graphite oxide. Carbon 2007;45(7):1558–65.
[22] Becerril HA, Mao J, Liu Z, Stoltenberg RM, Bao Z, Chen Y. Evaluation of solution-processed reduced graphene oxide films as transparent conductors. ACS Nano 2008;2(3):463–70.
[23] Hummers WS, Offeman RE. Preparation of graphitic oxide. J Am Chem Soc 1958;80(6):1339.
[24] Khan U, Porwal H, O'Neill A, Nawaz K, May P, Coleman JN. Solvent-exfoliated graphene at extremely high concentration. Langmuir 2011;27(15):9077–82.
[25] Ferrari AC, Basko DM. Raman spectroscopy as a versatile tool for studying the properties of graphene. Nat Nanotechnol 2013;8(4):235–46.
[26] Scaccia S, Goszczynska B. Sequential determination of platinum, ruthenium, and molybdenum in carbon-supported Pt, PtRu, and PtMo catalysts by atomic absorption spectrometry. Talanta 2004;63(3):791–6.
[27] Trejos T, Montero S, Almirall JR. Analysis and comparison of glass fragments by laser ablation inductively coupled plasma mass spectrometry (LA-ICP-MS) and ICP-MS. Anal Bioanal Chem 2003;376(8):1255–64.
[28] Zhang Y, Kang D, Saquing C, Aindow M, Erkey C. Supported platinum nanoparticles by supercritical deposition. Ind Eng Chem Res 2005;44(11):4161–4.
[29] Liu J, Cao J, Huang Q, Li X, Zou Z, Yang H. Methanol oxidation on carbon-supported Pt–Ru–Ni ternary nanoparticle electrocatalysts. J Power Sources 2008;175(1):159–65.
[30] Pu NW, Wang CA, Sung Y, Liu YM, Ger MD. Production of few-layer graphene by supercritical $CO_2$ exfoliation of graphite. Mater Lett 2009;63(23):1987–9.
[31] Ferrari A, Meyer J, Scardaci V, Casiraghi C, Lazzeri M, Mauri F, et al. Raman spectrum of graphene and graphene layers. Phys Rev Lett 2006;97(18):187401.
[32] Wang YY, Ni ZH, Yu T, Shen ZX, Wang HM, Wu YH, et al. Raman studies of monolayer graphene: the substrate effect. J Phys Chem C 2008;112(29):10637–40.
[33] Ferrari A, Robertson J. Interpretation of Raman spectra of disordered and amorphous carbon. Phys Rev B 2000;61(20):14095.
[34] Ferrari A. Raman spectroscopy of graphene and graphite: disorder, electron–phonon coupling, doping and nonadiabatic effects. Solid State Commun 2007;143(1):47–57.
[35] O'Neill A, Khan U, Nirmalraj PN, Boland J, Coleman JN. Graphene dispersion and exfoliation in low boiling point solvents. J Phys Chem C 2011;115(13):5422–8.
[36] Calizo I, Balandin A, Bao W, Miao F, Lau C. Temperature dependence of the Raman spectra of graphene and graphene multilayers. Nano Lett 2007;7(9):2645–9.
[37] Kudin KN, Ozbas B, Schniepp HC, Prud'Homme RK, Aksay IA, Car R. Raman spectra of graphite oxide and functionalized graphene sheets. Nano Lett 2008;8(1):36–41.
[38] Chen W, Yan L, Bangal P. Chemical reduction of graphene oxide to graphene by sulfur-containing compounds. J Phys Chem C 2010;114(47):19885–90.
[39] Tuinstra F, Koenig J. Characterization of graphite fiber surfaces with Raman spectroscopy. J Compos Mater 1970;4(4):492–9.
[40] Teweldebrhan D, Balandin AA. Modification of graphene properties due to electron-beam irradiation. Appl Phys Lett 2009;94(1):013101.
[41] Worsley MA, Pham TT, Yan A, Shin SJ, Lee JR, Bagge-Hansen M, et al. Synthesis and characterization of highly crystalline graphene aerogels. ACS Nano 2014;8(10):11013–22.
[42] Huang H, Chen H, Sun D, Wang X. Graphene nanoplate–Pt composite as a high performance electrocatalyst for direct methanol fuel cells. J Power Sources 2012;204:46–52.
[43] Shafiei M, Spizzirri PG, Arsat R, Yu J, Plessis J, Dubin S, et al. Platinum/graphene nanosheet/SiC contacts and their application for hydrogen gas sensing. J Phys Chem C 2010;114(32):13796–801.
[44] Frelink T, Visscher W, Cox AP, van Veen JAR. Ellipsometry and dems study of the electrooxidation of methanol at Pt and Ru- and Sn- promoted Pt. Electrochim Acta 1995;40(10):1537–43.
[45] Stamenkovic VR, Mun BS, Mayrhofer KJ, Ross PN, Markovic NM. Effect of surface composition on electronic structure, stability, and electrocatalytic properties of Pt-transition metal alloys: Pt-skin versus Pt-skeleton surfaces. J Am Chem Soc 2006;128(27):8813–9.
[46] Wakisaka M, Mitsui S, Hirose Y, Kawashima K, Uchida H, Watanabe M. Electronic structures of Pt–Co and Pt–Ru alloys for CO-tolerant anode catalysts in polymer electrolyte fuel cells studied by EC-XPS. J Phys Chem B 2006;110(46):23489–96.
[47] Balbuena PB, Subramanian VR. Theory and experiment in electrocatalysis. Springer; 2010.
[48] Lee S, Mukerjee S, Ticianelli E, McBreen J. Electrocatalysis of CO tolerance in hydrogen oxidation reaction in PEM fuel cells. Electrochim Acta 1999;44(19):3283–93.
[49] Lin W, Zei M, Eiswirth M, Ertl G, Iwasita T, Vielstich W. Electrocatalytic activity of Ru-modified Pt (1 1 1) electrodes toward CO oxidation. J Phys Chem B 1999;103(33):6968–77.
[50] Arico A, Baglio V, Di Blasi A, Modica E, Antonucci P, Antonucci V. Analysis of the high-temperature methanol oxidation behaviour at carbon-supported Pt–Ru catalysts. J Electroanal Chem 2003;557:167–76.
[51] Ren F, Wang C, Zhai C, Jiang F, Yue R, Du Y, et al. One-pot synthesis of a RGO-supported ultrafine ternary PtAuRu catalyst with high electrocatalytic activity towards methanol oxidation in alkaline medium. J Mater Chem A 2013;1(24):7255–61.
[52] Liu Z, Ling X, Su X, Lee JY. Carbon-supported Pt and PtRu nanoparticles as catalysts for a direct methanol fuel cell. J Phys Chem B 2004;108(24):8234–40.
[53] Park KW, Ahn KS, Nah YC, Choi JH, Sung YE. Electrocatalytic enhancement of methanol oxidation at Pt-WOx nanophase electrodes and in situ observation of hydrogen spillover using electrochromism. J Phys Chem B 2003;107(18):4352–5.
[54] Liang Y, Zhang H, Tian Z, Zhu X, Wang X, Yi B. Synthesis and structure–activity relationship exploration of carbon-supported PtRuNi nanocomposite as a CO-tolerant electrocatalyst for proton exchange membrane fuel cells. J Phys Chem B 2006;110(15):7828–34.
[55] Yang D, Velamakanni A, Bozoklu G, Park S, Stoller M, Piner RD, et al. Chemical analysis of graphene oxide films after heat and chemical treatments by X-ray photoelectron and Micro-Raman spectroscopy. Carbon 2009;47(1):145–52.
[56] Hsin YL, Hwang KC, Yeh CT. Poly(vinylpyrrolidone)-modified graphite carbon nanofibers as promising supports for PtRu catalysts in direct methanol fuel cells. J Am Chem Soc 2007;129(32):9999–10010.
[57] Wu B, Hu D, Kuang Y, Liu B, Zhang X, Chen J. Functionalization of carbon nanotubes by an ionic-liquid polymer: dispersion of Pt and PtRu nanoparticles on carbon

nanotubes and their electrocatalytic oxidation of methanol. Angew Chem Int Ed 2009;48(26):4751–4.
[58] Mu Y, Liang H, Hu J, Jiang L, Wan L. Controllable Pt nanoparticle deposition on carbon nanotubes as an anode catalyst for direct methanol fuel cells. J Phys Chem B 2005;109:22212–6.
[59] Guo S, Dong S, Wang E. Polyaniline/Pt hybrid nanofibers: high-efficiency nanoelectrocatalysts for electrochemical devices. Small 2009;5(16):1869–76.
[60] Li Y, Tang L, Li J. Preparation and electrochemical performance for methanol oxidation of Pt/graphene nanocomposites. Electrochem Commun 2009;11(4):846–9.
[61] Nethravathi C, Anumol EA, Rajamathi M, Ravishankar N. Highly dispersed ultrafine Pt and PtRu nanoparticles on graphene: formation mechanism and electrocatalytic activity. Nanoscale 2011;3:569–71.
[62] Guo S, Dong S, Wang E. Three-dimensional Pt-on-Pd bimetallic nanodendrites supported on graphene nanosheet: facile synthesis and used as an advanced nanoelectrocatalyst for methanol oxidation. ACS Nano 2010;4(1):547–55.
[63] Li Y, Gao W, Ci L, Wang C, Ajayan PM. Catalytic performance of Pt nanoparticles on reduced graphene oxide for methanol electro-oxidation. Carbon 2010;48(4):1124–30.
[64] Yadav A, Nishikata A, Tsuru T. Effect of halogen ions on platinum dissolution under potential cycling in 0.5M $H_2SO_4$ solution. Electrochim Acta 2007;52(26):7444–52.
[65] Yuan H, Guo D, Qiu X, Zhu W, Chen L. Influence of metal oxides on Pt catalysts for methanol electrooxidation using electrochemical impedance spectroscopy. J Power Sources 2009;188(1):8–13.
[66] Wang ZB, Yin GP, Shao YY, Yang BQ, Shi PF, Feng PX. Electrochemical impedance studies on carbon supported PtRuNi and PtRu anode catalysts in acid medium for direct methanol fuel cell. J Power Sources 2007;165(1):9–15.